Acute inhibition of transient receptor potential vanilloid-type 4 cation channel halts cytoskeletal dynamism in microglia

BEEKEN, Jolien; MERTENS, Melanie; Stas, Nathan; KESSELS, Sofie; AERTS, Liese; JANSSEN, Bieke; Mussen, Femke; Pinto, Silvia; Vennekens , Rudi; RIGO, Jean-Michel; Nguyen, Laurent; BRONE, Bert & AGUIAR ALPIZAR, Yeranddy (2022)
Acute inhibition of transient receptor potential vanilloid-type 4 cation channel halts cytoskeletal dynamism in microglia. In: Glia , 70 (11) , p. 2157-2168.

DOI: 10.1002/glia.24243
Handle: http://hdl.handle.net/1942/37951

Acute inhibition of transient receptor potential vanilloid-type 4 cation channel halts cytoskeletal dynamism in microglia

Running title: TRPV4 inhibition hinders microglial dynamism

Jolien Beeken[1,2], Melanie Mertens[1], Nathan Stas[1], Sofie Kessels[1], Liese Aerts[1], Bieke Janssen[1], Femke Mussen[1], Silvia Pinto[3], Rudi Vennekens[3], Jean-Michel Rigo[1], Laurent Nguyen[2], Bert Brône[1†], Yeranddy A. Alpizar[1†]

[1] Hasselt University, BIOMED, Diepenbeek, Belgium

[2] Université de Liège, GIGA-Stem-Cells, Liège, Belgium

[3] Laboratory for Ion Channel Research, VIB-KU Leuven, Leuven, Belgium

† These authors contributed equally to this work as co–senior authors

Correspondence to:

Yeranddy A. Alpizar email: yeranddy.aguiaralpizar@uhasselt.be

Bert Brône email: bert.brone@uhasselt.be

ACKNOWLEDGEMENTS

We thank Melissa Jans and Yennick Geuens for the maintenance of the mouse colonies at BIOMED; Rosette Beenaerts and Petra Bex for their technical assistance with genotyping and cell culture maintenance; and Dr. Sam Duwé from the Advanced Optical Microscopy Centre for training, support and access to the instrumentation. The graphical abstract was created in BioRender.com.

J.B. is a PhD student supported by the Special Research Foundation (BOF17DOCLI01) from Hasselt University and Université de Liège. M.M. is a PhD student supported by the Special Research Foundation UHasselt (BOF21DOC21). Y.A.A is supported by an FWO senior postdoctoral fellowship (12H8220N). This work was supported by FWO research grants (1521619N), Special Research Foundation UHasselt (BOF16NI04, BOF20KP11, BOF21KP06, BOF21GP05), Sint Gillis autism research grant, the ROTARY Espoir en Tête – Hoofdzaak er is Hoop, the F.R.S.-F.N.R.S. (Synet; EOS 0019118F-RG36), the Fonds Leon Fredericq, the Fondation Médicale Reine Elisabeth, the Fondation Simone et Pierre Clerdent, the Belgian Science Policy (IAP-VII network P7/20), and the ERANET Neuron STEM-MCD and NeuroTalk.

AUTHOR CONTRIBUTIONS

B.B. and Y.A.A conceived and designed the project. J.B., M.M., S.K. and Y.A.A. designed or conducted the *ex vivo* branch motility experiments. J.B., M.M. and Y.A.A. conducted microglial morphology and density experiments. J.B., L.A. and Y.A.A. performed and quantified the *in vitro* random walk. J.B., N.S., B.J., F.M. and Y.A.A. isolated and cultured primary microglia and conducted the *in vitro* morphology and motility experiments. J.B. contributed with the analysis of all experiments. N.S., J.B., M.M. and Y.A.A. conducted and quantified the tubulin and filopodia imaging experiments. S.P. and R.V. provided the *Trpv4* KO mice. All authors contributed to the interpretation of data. J.B. and Y.A.A. wrote the manuscript with input from all co-authors.

CONFLICT OF INTEREST

The authors declare no competing interests.

Word count (total): 5118

ABSTRACT (Word count: 193)

Microglia, the resident macrophages of the central nervous system are highly motile cells that support brain development, provision neuronal signaling and protect brain cells against damage. Proper microglial functioning requires constant cell movement and morphological changes. Interestingly, the transient receptor potential vanilloid 4 (TRPV4) channel, a calcium-permeable channel, is involved in hypoosmotic morphological changes of retinal microglia and regulates temperature-dependent movement of microglia cells both *in vitro* and *in vivo*. Despite the broad functions of TRPV4 and the recent findings stating a role for TRPV4 in microglial movement, little is known about how TRPV4 modulates cytoskeletal remodeling to promote changes of microglial motility. Here we show that acute inhibition of TRPV4, but not its constitutive absence in the *Trpv4* KO cells, affects the morphology and motility of microglia *in vitro*. Using high-end confocal imaging techniques, we show a decrease in actin-rich filopodia and tubulin dynamics upon acute inhibition of TRPV4 *in vitro*. Furthermore, using acute brain slices we demonstrate that *Trpv4* knockout microglia display lower ramification complexity, slower process extension speed and consequently smaller surveyed area. We conclude that TRPV4 inhibition triggers shifts in cytoskeleton remodelling of microglia influencing their migration and morphology.

KEYWORDS

Microglia, TRPV4, Cytoskeleton, Morphology, Random persistent walk, Process motility

MAIN POINTS

- Acute inhibition of TRPV4 abrogates microtubule and actin-rich filopodia dynamism in microglia *in vitro*.
- *Trpv4* KO microglia exhibit less ramification complexity and slower process extension speed *in situ*.

DATA AVAILABILITY STATEMENT

Data available on request from the authors.

1. INTRODUCTION (Word count: 699)

Microglia, the resident immune cells of the central nervous system (CNS), play an essential role during development and homeostasis (Smolders *et al.*, 2019; Wolf *et al.*, 2017). They mediate brain homeostasis by maintaining neuronal networks, stimulating tissue repair as well as eliminating dead or damaged cells, intruding pathogens and redundant synapses via phagocytosis (Colonna & Butovsky, 2017; Salter & Stevens, 2017; Wolf *et al.*, 2017). For proper functioning, microglia require constant movement either through process motility or migration, events that are highly dependent on cytoskeletal rearrangements (Nimmerjahn *et al.*, 2005; Wolf *et al.*, 2017). It has been widely established that cytoskeleton remodeling is induced through a molecular machinery consisting of membrane receptors (e.g., ion channels, integrins) which allow the cell to sense environmental changes, hereby regulating cell responses (Franco-Bocanegra *et al.*, 2019; Madry & Attwell, 2015; Nimmerjahn *et al.*, 2005; Ohsawa & Kohsaka, 2011). Although several ion channels have been shown to mediate protrusion formation and migration in microglia (Hines *et al.*, 2009; Smolders *et al.*, 2019; Swiatkowski *et al.*, 2016), the molecular signaling pathways underpinning cytoskeleton remodeling in microglia remain largely unknown.

Recent *in vivo* research showed that microglial processes mainly exhibit Ca^{2+} signaling in their protruding branches without significant fluctuations in somatic Ca^{2+} levels (Umpierre *et al.*, 2020). Noteworthy, local Ca^{2+} increases necessary for cell dynamics and movement are not solely initiated by chemoattractant signal transduction but also by stretch-activated calcium-permeable channels from the transient receptor potential (TRP) channel family (Wei *et al.*, 2009).

TRP channels are involved in a variety of physiological processes such as nociception, proprioception and thermosensation (Canales *et al.*, 2019; Liu & Montell, 2015; Nilius & Owsianik, 2011). They have a key function in cellular processes such as volume regulation, proliferation, activation and cell death (Becker *et al.*, 2005; Clapham, 2003; Echeverry *et al.*, 2016; Ryskamp *et al.*, 2016). Several Ca^{2+}-permeable TRP channels are expressed in microglial cells and have been reported to play a pivotal role in regulating their function (Chakraborty & Goswami, 2022; Echeverry *et al.*, 2016; Konno *et al.*, 2012; Mizoguchi *et al.*, 2014; Nishimoto *et al.*, 2021; Sappington & Calkins, 2008; Sun *et al.*, 2014). For example, TRPV1 is mainly associated with neurotoxicity as it is involved in the release of proinflammatory cytokines by microglia (Echeverry *et al.*, 2016). On the other hand, TRPM2 is essential for the temperature-dependent movement of microglia as well as stress-induced activation (Echeverry *et al.*, 2016; Nishimoto *et al.*, 2021), while TRPC3 contributes to microglial activation through the suppression of brain-derived neurotrophic factor (BDNF) (Mizoguchi *et al.*, 2014). More recently, TRPV4 has been implicated in the regulation of microglial morphology and intracellular signaling in response to hypoosmotic conditions (Redmon *et al.*, 2021) and temperature-dependent motility (Nishimoto *et al.*, 2021). However, the role of TRPV4 in cytoskeletal regulation aiding microglial motility remains elusive. Interestingly, TRPV4 is involved in regulating cytoskeleton rearrangements in endometrial cancer cells by mediating Ca^{2+}-influxes (Li *et al.*, 2020). In neurons a direct interaction of TRPV4 is shown with actin, tubulin and neurofilament proteins through its C-terminus. The receptor colocalized with actin-rich structures such as filopodia, lamellipodia and focal adhesion points, thereby regulating cell morphology and net movement of neurites (Goswami *et al.*, 2010). In astrocytes, TRPV4 influences intracellular pathways involved in the astrocytic end-feet while in endothelial cells, the cytoskeleton regulates Ca^{2+}-influx through

TRPV4 (Kanju & Liedtke, 2016). TRPV4 is involved in macrophage phagocytosis and foam cell formation, two processes highly dependent on Ca^{2+}-signaling (Dutta *et al.*, 2020; Michalick & Kuebler, 2020). It should be noted that TRPV4 activity can be modified by alterations in cell swelling, stretch, shear flow, plasma membrane phospholipids or the actin cytoskeleton (Canales Coutino & Mayor, 2021; Liu & Montell, 2015), hereby it is likely that the channel regulates cell motility through Ca^{2+}-mediated mechanotransduction. Here, we assessed the effects of acute TRPV4 inhibition on microglial morphology, movement and cytoskeleton dynamics. We found that acutely-inhibiting TRPV4 increases circularity of primary cultured microglia while it decreases area and total displacement. Furthermore, we showed that cytoskeletal dynamics are decreased upon inhibition of TRPV4 *in vitro*. Even though constitutive absence of TRPV4 did not alter morphology *in vitro*, we found significant decreases in morphological complexity and brain surveillance *in situ*.

2. MATERIALS AND METHODS (Word count: 1818)

2.1 Animals

All animal experiments were conducted in accordance with the European Community guiding principles on the care and use of animals and with the approval of the Ethical Committee on Animal Research of Hasselt University. Animals were group-housed in a temperature and humidity-controlled room with *ad libitum* access to food and water and a 12 h light-dark cycle. CX3CR1$^{eGFP/+}$ *Trpv4* knockout (KO) and CX3CR1$^{eGFP/+}$ wild type (WT) littermates used in this study were obtained by breeding heterozygous *Trpv4* (*Trpv4*$^{+/-}$) with CX3CR1$^{eGFP/eGFP}$ *Trpv4*$^{+/-}$ mice. *Trpv4* KO mice were kindly provided by the Laboratory for Ion Channel Research at KU Leuven. CX3CR1$^{eGFP/eGFP}$ (Jung *et al.*, 2000) mice were obtained from the European Mouse Mutant Archive (EMMA) Institute with the approval of Steffen Jung (Weizmann Institute of Science). For all experiments, mice of either sex were age-matched and combined with littermate controls.

2.2 Primary microglia isolation

Cortical microglia from CX3CR1$^{eGFP/+}$WT and CX3CR1$^{eGFP/+}$*Trpv4* KO mice were isolated following experimental procedures described elsewhere (Stark *et al.*, 2018). In brief, brains of postnatal day 21 (P21) mice were dissected and the midbrain, cerebellum and meninges were carefully removed. The remainder of the brain was disintegrated in Dulbecco's Modified Eagle's Medium (DMEM, Sigma-Aldrich, Overijse, Belgium) supplemented with 1% penicillin/streptomycin (P/S, Invitrogen, Merelbeke, Belgium), followed by incubation with papain (17 U/mg, Sigma-Aldrich) and DNase I (10 mg/ml, Roche, Brussel, Belgium) for 30 min at 37 °C. Cell suspensions were filtered through a 70 µm cell strainer, centrifuged (5 min, 500 x g) and pellets were resuspended in DMEM containing 30% stock isotonic Percoll (SIP, GE Healthcare, Diegem, Belgium). Hereafter, a density gradient was created by the addition of 70% SIP diluted in PBS and the suspension was centrifuged for 25 min at 650 x g (brake 0, acceleration 4). The cell cloud at the interphase between 30% and 70% was collected, diluted in 10 ml cold PBS and centrifuged for 10 min at 500 x g. Cell pellets were resuspended in magnetic-activated cell sorting (MACS) buffer (2 mM EDTA and 0.5% fetal calf serum (FCS)) and microglia were isolated by positive selection using CD11b microbeads (Miltenyi Biotec, Gladbach, Germany), following the manufacturer's instructions. CD11b^{+} cells were resuspended in DMEM supplemented with 10% FCS, 10% horse serum (Thermofisher, Waltham, MA, US) and 1% P/S (DMEM 10:10:1) and seeded onto glass coverslips (30 x 10^3 cells/well), 24-well plates (30 x 10^3 cells/well), or 35 mm MatTek glass bottom dishes (10^5 cells/dish, MatTek, Ashland, MA, US) pre-coated with poly-D-lysine (PDL, 20 µg/ml, Gibco, Waltham, MA, US) and collagen type IV (2 µg/ml, Sigma-Aldrich), and incubated in a humidified incubator at 37 °C, 8.5% CO_2 for 7 days. Afterwards, a dynamic ramified morphology was induced by the addition of serum-free medium (hereafter, TIC medium (Bohlen *et al.*, 2017)) containing 5 µg/ml insulin, 5 µg/ml N-acetyl-cysteine, 100 µg/ml apo-transferrin, 0.1 µg/ml Na_2SeO_3, 1 µg/ml heparan sulfate, 2 µg/ml human TGF-ß2 (PeproTech, Rocky Hill, NJ, US), 0.1 µg/ml murine IL-34 (BioLegend, Amsterdam, The Netherlands), 1.5 µg/ml ovine wool cholesterol, 3 µg/ml L-glutamine in DMEM/F12. For all experiments, cells were seeded 7 days in DMEM 10:10:1 medium followed by 3-7 days TIC medium unless stated otherwise.

For quantification of microglial morphology *in vitro*, images were processed using Fiji software (Schindelin *et al.*, 2012) by manually defining cell contours and quantifying area and perimeter. Circularity was calculated as $4\pi\frac{Area}{Perimeter^2}$, where a value of 1 indicates a perfect circle.

2.3 Live-cell tubulin imaging

$CD11b^+$ cells cultured in 24-well glass bottom plates (Ibidi, Gräfelfing, Germany) (30 x 10^3 cells) or glass bottom dishes (10^4 cells) were incubated with SiR-Tubulin (1 µM, 45 min, Spirochrome, Thurgau, Switzerland) at 37 °C. Afterwards, cells were rinsed and imaged before and after being exposed to solutions containing GSK2193874 (10 µM) or GSK1016790A (300 nM, Tocris Bioscience, Bristol, United Kingdom) prepared in Krebs (in mM: 150 NaCl, 6 KCl, 10 HEPES, 10 glucose, 1.5 $CaCl_2$, 1 $MgCl_2$, pH 7.4) either manually or via perfusion by gravity using a multi-barrelled pipette tip. Live cell tubulin images were obtained using the 100X oil objective followed by structured illumination microscopy processing on the Zeiss Elyra PS1 and analyzed using the PIVlab toolbox (Thielicke & Stamhuis, 2014) in MATLAB release 2021a (9.10.0.1649659). For analysis, contrast was enhanced using a contrast-limited adaptive histogram equalization (set at 20 px) and denoised (set at 3 px) using pre-processing built-in options. Particle displacements were quantified using a FFT window deformation algorithm in interrogation areas of 32 pixels (pass 1) and 16 pixels (pass 2). Velocity vectors were filtered to exclude low contrast areas and heat maps representing velocity magnitudes were generated to include all values of the control condition.

2.4 Filopodia motility

$CD11b^+$ cells were cultured in a 24-well glass bottom plate (3 x 10^4 cells/well) and imaged during a time series before and after exposure to a GSK2193874 (10 µM) solution prepared in Krebs. Confocal images were obtained using the optimal pinhole size for the 63X oil objective on the Zeiss LSM880-Airyscan. All images were processed using Fiji software. For analysis and quantification of filopodia motility, each slice of every stack was filtered (median = 2), thresholded and binarized. To visualize filopodia, a region of interest in between main processes (ROImp) was manually drawn and data outside this region was erased. Maximum intensity projections were performed and cumulative filopodia positions (surveyed area) were calculated as the area of maximum intensity pixels within the ROImp. For quantification of filopodia length, each filopodium was manually tracked using the segmented line tool.

2.5 Persistent random walk

$CD11b^+$ cells were cultured in DMEM 10:10:1 medium on pre-coated coverslips (30 x 10^3 cells) as described before. After 5 days in culture, cells were imaged every 15 min for a total duration of 24 h using an Incucyte S3 (Essen BioScience, Newark, United Kingdom). Persistent random walk and mobility analysis were assessed using Fiji software. Microglial migration, defined as displacement of the cell body, was manually tracked in 2D for 6 h using the MTrackJ plugin (Meijering *et al.*, 2012) while the percentage of motile cells was calculated by manually counting the total number cells with at least one soma displacement event > 10 µm over 10 h.

2.6 Brain perfusion, immunofluorescence and imaging

Wild type CX3CR1$^{eGFP/+}$ and CX3CR1$^{eGFP/+}$ *Trpv4* KO mice were anesthetized at P21 by intraperitoneal injection of 2.5 mg/g (body weight) of Dolethal. Mice were transcardially perfused with cold PBS containing heparin (20 I.U.; Heparine LEO 5.000 I.U./ml, Lier, Belgium) followed by 4% cold paraformaldehyde (PFA). Brains were dissected and incubated in 4% PFA overnight at 4 °C, washed with PBS and kept in PBS-azide (0.01%) until slicing. Free-floating sections (100 µm) were cut using a Microm HM650V Vibratome (Prosan, Monheim, Germany) and stained with DAPI (Sigma-Aldrich) for 15 min. The sections were mounted on microscope slides (ThermoScientific) and coverslipped in fluorescent mounting medium (Immu-Mount, ThermoScientific). To investigate morphology or volumetric density, cortical sections were imaged using a confocal microscope (Zeiss LSM880) and eGFP$^+$ microglia were visualized using the Argon 488 nm laser. Microglial cells were captured within a 20 µm z-stack, stepping 1 µm using a 63X oil objective (NA 1.4). For surface density analysis, cortical brain sections were imaged using an automated slide scanner (Zeiss AxioScan.Z1) with 20X objective.

2.7 Sholl and density analysis

Microglial morphology was assessed by Sholl analysis, as described by Kyrargyri *et al.* (Kyrargyri *et al.*, 2020). In brief, cell reconstructions were performed using 3D automatic cell tracing in Vaa3D software (http://www.vaa3D.org) using the APP2 (All-path-pruning 2.0) algorithm to generate 3D skeletons of the ramified microglia (Xiao & Peng, 2013). The morphological features were analyzed using a length-based hierarchical pruning method, as previously described by (Kyrargyri *et al.*, 2020). Custom codes in MATLAB are available at https://github.com/AttwellLab/Microglia. Microglial density was quantified in the secondary motor cortex layer 1, 2/3 and 5 by calculating the number of cells per area unit (mm^2). Analyses were carried out with experimenters blinded to the genotype.

2.8 Two-photon imaging of acute brain slices

P21 mice were sacrificed by decapitation followed by quick brain dissection in oxygenated ice-cold slicing solution containing (in mM): 120 N-methyl-d-glucamine, 2.5 KCl, 25 $NaHCO_3$, 1 $CaCl_2$, 7 $MgCl_2$, 1.2 NaH_2PO_4, 20 D-glucose, 2.4 Na^+ pyruvate, 1.3 Na^+-L-ascorbate, pH 7.3-7.4, ~300 mOsm. Brains were coronally sliced (300 µm-thick) using a vibratome (LEICA VT1200S) and allowed to recover for 1 h at 36 °C in oxygenated artificial CSF (aCSF) containing (in mM): 126 NaCl, 2.5 KCl, 26 $NaCHO_3$, 2 $CaCl_2$, 2 $MgCl_2$, 1.25 NaH_2PO_4, 10 D-glucose, pH 7.3-7.4, ~300 mOsm. Experiments were performed under continuous perfusion of oxygenated (95% O_2 and 5% CO_2) aCSF at room temperature to preserve slice health.

Acute brain slice imaging was performed using a Zeiss LSM880-Airyscan confocal microscope (with a 40X EC plan-Neofluar objective, NA 1.4) provided with a Mai Tai DeepSee Ti:Sapphire-pulsed laser (Spectra-Physics, Utrecht, The Netherlands) tuned at 920 nm (13 mW intensity, 1.54 µs pixel dwell). Stacks were recorded starting from a minimal depth of 50 µm above the surface of the slice to avoid cells being activated by slicing (Eyo *et al.*, 2014; Schiefer *et al.*, 1999).

For branch motility analysis, a z-stack spanning 14 µm with serial optical sections every 1 µm was acquired every minute during 10 min.

2.9 Acute brain slice image processing

All images were processed as described before (Bernier *et al.*, 2019; Kyrargyri *et al.*, 2020) using Fiji software. For analysis and quantification of microglial surveillance, each slice of every stack was filtered (median filter = 1) followed by subtraction of background with a ball size of 30. The 3D-stacks were then registered for drifting by applying the StackReg plugin with rigid body transformation (Thevenaz *et al.*, 1998). Maximum intensity projections were performed and individual cells were selected by manually drawing a region of interest and erasing data outside this region. These individual cells were then manually binarized by applying Huang threshold which is based on the intensity and morphology of the cell. Threshold values were set ensuring the presence of all microglial processes in all the different frames. To quantify surveillance, for each movie, consecutive binarized images were pairwise subtracted to generate a new movie consisting of pixels that represent moving processes. Surveyed area was then calculated as the sum of these pixels over a time span of 10 min. Extension and retraction speed of microglial processes were calculated by tracking individual branches using the MTrackJ plugin (Meijering *et al.*, 2012) for a total duration of 10 min.

2.10 Statistical analysis

Statistical analysis and graphs were produced using Prism 9 (GraphPad Software) and OriginPro 9.0.0 (OriginLab, Northampton, MA, US). Data distributions were assessed for normality (Shapiro-Wilk) and parametric or non-parametric two-tailed tests were applied accordingly. The reader is referred to the figure legends for details about the sample size and specific statistical analysis. Box graphs represent median (middle line) and SD (box length). Individual data points are shown in light gray. *P* values smaller than 0.05 were considered significant.

3. RESULTS (Word count: 1448)

3.1 TRPV4 regulates microglial morphology and motility *in vitro*

First, we sought to determine the contribution of basal TRPV4 activity in the regulation of microglial morphology *in vitro*. To recapitulate the phenotype of microglial cells *in vivo*, we used a combination of survival-promoting cues (TGF-β2, IL-34, and cholesterol) in serum-free medium (TIC medium (Bohlen *et al.*, 2017)). Under this condition, cultured microglia from wild type (WT) animals are highly ramified, exhibiting a small cell body and long thin processes with filopodia (**Figure 1a, Figure 3a**). We assessed the morphological differences with cultured microglia from *Trpv4* knockout (KO) mice by quantifying cell shape (circularity) and size (area). Interestingly, the morphological complexity of microglia remained unchanged in cells with a constitutive deficiency of TRPV4 (*Trpv4* KO), with cells equally abundant in ramifications (low circularity values) and similar cellular area (**Figure 1a, b**).

Next, we examined the effect of acute inhibition of TRPV4 activity on microglial morphology. For this, we analyzed the morphological features using live-cell imaging on WT primary microglia treated with different concentrations of three TRPV4 antagonists, namely GSK2193874 (hereafter GSK21), HC067047 (HC) and RN9893 (RN). Whereas vehicle (0.2% DMSO)-treated microglia remained highly ramified and motile over time (up to 48 hours), with no significant changes in circularity and area, acute inhibition of TRPV4 with GSK21 and HC compounds induced a shortening of main branches and thin ramifications, and prevented cell migration during 24 h treatment with the TRPV4 antagonist (**Figure 1c-e, Figure S1a, b**). Quantitative analysis of morphological parameters revealed that microglia treated with 10 µM GSK21 and HC show significant increased circularity and reduced area as fast as 30 min after TRPV4 inhibition. In contrast, acute inhibition with RN evoked a short-lasting decrease of cellular area, with no significant effect in cell circularity.

Changes in morphological complexity of microglia treated with a 10 times lower dose of GSK21 were only evident after 48 h (**Figure 1e**), indicating that TRPV4 inhibition induces branch retraction in a time- and concentration-dependent manner. Conversely, the effects induced by GSK21 and RN were significant up to 6 h, with cells recovering their morphological complexity by 24 h incubation time.

In addition, acute inhibition of TRPV4 activity with 10 µM GSK21 and HC decreased the percentage of microglia exhibiting non-directed migration and the total displacement during persistent random walk (**Figure 1d, f, g, Figure S1c**). GSK21 (1 µM) was less effective in reducing microglial persistent random walk, likely a consequence of the late effect on the morphological changes (**Figure 1e, g**). The transient effect of RN compound did not alter the overall non-directed migration of microglia (**Figure S1c**).

Possible off-target effects from the TRPV4 antagonist were evaluated by comparing morphological and migratory effects in *Trpv4* KO microglia untreated and treated with GSK21, HC and RN (10 µM). No significant differences were observed on morphology nor percentage of motile cells and total displacement during persistent random walk (**Figure S2**). Taken together, our results show that inhibition of TRPV4, but not constitutive absence, reduces microglial process complexity, area and overall migration *in vitro*.

3.2 TRPV4 inhibition reduces microglial tubulin and actin-rich filopodia dynamics *in vitro*

TRPV4 activity regulates cytoskeletal changes in neuronal cells by directly interacting with microtubules (MT) and actin, thus modifying cell morphology and motility (Goswami *et al.*, 2010). However, whether similar functional interactions operate in microglia remains to be elucidated. To evaluate this, we investigated tubulin and actin-rich filopodia dynamics before and after exposure to the TRPV4 antagonist. First, we used the cell-permeable fluorescent dye SiR-Tubulin to label the MTs of WT microglia untreated and treated with GSK21 (10 µM). Live-cell super-resolution microscopy revealed highly dynamic MTs in untreated primary microglia (**Supplementary movie 1**). Moreover, overlaying consecutive regions of MTs from WT microglia (5 s apart), clearly showed fast MT displacement over time (**Figure 2a, top left panel**). To further quantify this dynamism, we used particle image velocimetry (PIV) which allowed for measuring cross correlations in pixel intensity between regions of two consecutive images in a defined time frame (interrogation area). PIV analysis provides a range of vector velocities for the selected interrogation areas (**Figure 2b, white bar**) representing the displacement of MTs, as shown in the heatmap of **Figure 2a**. Upon inhibition of TRPV4, MT dynamism was abrogated (**Figure 2a top right panel, Supplementary movie 2**), with a decreased vector velocity over one frame compared to the untreated cells (**Figure 2b**). Quantification of the total time-lapse revealed a reduced cumulative vector velocity in specific interrogation areas for microglia with acute TRPV4 inhibition, demonstrating the sustained effect of TRPV4 inhibition over tubulin dynamism (**Figure 2c**). Furthermore, we observed that untreated microglia exhibit a greater median velocity per frame compared to GSK21-treated microglia (**Figure 2d**), indicating a reduction in MT displacement over the entire timespan. Overall, these data show altered MT dynamics after acutely-inhibiting TRPV4 in primary microglia.

Next, we determined whether the TRPV4 antagonist also affects filopodia dynamics. Since filopodia are actin-rich structures (Franco-Bocanegra *et al.*, 2019), their dynamical changes are indicative for the effect of acute TRPV4 inhibition on microglial actin dynamics. We took advantage of the ubiquitous expression of eGFP in our CX3CR1-eGFP mice to visualize the highly dynamic filopodia (Gallop, 2020). To assess filopodia number, length and movement, we defined multiple regions of interest surrounding microglial processes and recorded moving filopodia over a timespan of 2.5 min. TIC-cultured WT microglia were highly ramified and contained up to fourth order branches that were enriched with long and highly dynamic filopodia (**Figure 3a, left panel**). Upon treatment with GSK21 (10 µM), the morphological architecture of the main branches remained unaltered (for the extent of this experiment 2.5 min) (**Figure 3a, right panel**); however, a significant decrease in the number of filopodia (**Figure 3b**) and their corresponding length (**Figure 3c**) was observed. Filopodia movement was also reduced after exposure to GSK21 (**Figure 3c & Supplementary movie 3)**. Similarly, acute inhibition with HC and RN compounds decreased the length, number and motility of thin filopodia structures (**Figure S3**). Altogether, acute inhibition of TRPV4 significantly reduced filopodia features (**Figure 3b, c**), which subsequently decreased the area scanned by these structures (**Figure 3e**). In summary, these findings demonstrate that inhibition of TRPV4 reduces cytoskeletal rearrangements in microglia by decreasing dynamics of both tubulin and actin-rich filopodia.

3.3 *Trpv4* knockout affects microglial morphology and branch motility *in situ*

Unlike acute TRPV4 inhibition, *Trpv4* KO primary microglia exhibit migratory and morphological features *in vitro* that are undistinguishable from WT cells (**Figure 1a, 1b**). It should be noted that microglia lose part of their gene signature upon isolation from their brain (Bohlen *et al.*, 2017; Haynes *et al.*, 2006). Hereby, microglial function can slightly differ *in vitro* compared to *in situ*. We sought to test whether constitutive absence of TRPV4 could affect morphology, density and branch motility of microglia when present in their natural environment. We thus investigated branch motility using two-photon live-imaging of CX3CR1-eGFP microglia in acute cortical slices from WT and *Trpv4* KO mice. We quantified the surveyed area and both process extension and retraction speeds for total duration of 10 min. These experiments revealed highly dynamic WT microglia continuously scanning the environment, as represented in the overlaying time consecutive images in **Figure 4a**. Although *Trpv4* KO microglia displayed dynamic branches, we observed that the branches covered significantly less area during the same time lapse (2 min) (**Figure 4a, b**). To discern if the impact on brain area coverage resulted from changes in process motility, we quantified extension and retraction events by manually tracking motile processes from both WT and *Trpv4* KO microglia. We observed that retraction speed was not affected between both genotypes; however, lack of TRPV4 did significantly decrease process extension speed (**Figure 4c**).

Next, we probed for possible contributions in microglial density and morphological complexity after constitutive loss of TRPV4. We perfusion-fixed P21 WT and *Trpv4* KO mice and quantified microglial density in layers 1, 2/3 and 5 of the primary and secondary motor areas. Both WT and *Trpv4* KO mice exhibited a homogenous distribution of microglia throughout the brain, with no differences observed between both genotypes (**Figure 5a, b**). Finally, we analyzed microglia process ramification in the cortex by performing a three-dimensional Sholl analysis, from which the outcoming cell skeletons of *Trpv4* KO microglia showed an aberrant reduction in morphological complexity (**Figure 5c**). High-resolution confocal microscopy confirmed these changes and revealed a reduced ramification and number of tips in microglia lacking TRPV4 (**Figure 5d**). Furthermore, Sholl quantification displayed fewer branching points and shorter processes in *Trpv4* KO microglia compared to their WT littermates (**Figure 5e**). Thus, in contrast to density, *in situ* microglia lacking TRPV4 exhibit a reduced process extension speed, likely contributing to both a decreased process complexity and brain surveillance.

4. DISCUSSION (Word count: 960)

In microglia, Ca^{2+}-driven cell movement has been proven to be pivotal for proper brain development and maintaining homeostasis (Sharma & Ping, 2014); however, the mechanisms behind this process remain unknown. Recently, microglial TRPV4 was shown to be involved in the signaling and morphological changes in response to hypoosmotic conditions and pharmacological modulators (Chakraborty & Goswami, 2022; Redmon *et al.*, 2021) and temperature-dependent movement of microglia both *in vitro* and *in vivo* (Nishimoto *et al.*, 2021). Despite this increasing role for TRPV4 in microglia, its role on cytoskeleton remodeling necessary for microglial architecture and motility remains to be elucidated. Using live-cell imaging techniques *in vitro* and *in situ*, we here confirmed that TRPV4 activity regulates microglial morphology and migration. More importantly, we demonstrate that acute inhibition of TRPV4 directly affect remodeling of actin and tubulin cytoskeleton in microglia.

Using three different antagonists we demonstrate that acute TRPV4 inhibition evokes immediate changes in microglial morphology and branch motility. However, inhibition-induced long-lasting effects were variable among the compounds, most likely dependent on individual inhibition potency, solubility and stability properties.

To get insight into the possible mechanisms underpinning microglial motion, we analyzed tubulin and actin-rich filopodia dynamics before and after acute inhibition of TRPV4. Pharmacological inhibition of TRPV4 caused a significant decrease in both tubulin- and actin-dependent motion showing less dynamic MTs and decreased filopodia number and length. Consistent with these data, we found that acute inhibition of TRPV4 significantly reduced the area scanned by filopodia, a result correlated with the decreased filopodia features.

Our findings raise the question on how the channel can steer cytoskeleton remodeling in microglial cells. In light of previous studies, we speculate that the TRPV4-mediated Ca^{2+} influx contributes to the upregulation and recruitment of proteins necessary for cytoskeleton remodeling (Sharma & Ping, 2014; Tsai *et al.*, 2015; Tsai & Meyer, 2012; Wei *et al.*, 2009). Similar mechanisms are found in endometrial cancer cells, for instance, where TRPV4 regulates cytoskeleton rearrangements by mediating Ca^{2+}-influxes that activate the RhoA/ROCK1 pathway which in turn upregulates F-actin and paxillin, an actin-binding protein (Li *et al.*, 2020). On the other hand, TRPV4 activity promotes the activation of Rac1, a small GTPase involved in cell migration, by targeting AKT phosphorylation and thereby enhancing glioma cell motility (Ou-Yang *et al.*, 2018). Importantly, TRPV4 interacts directly with actin, tubulin and neurofilament proteins through its C-terminus, and the receptor colocalizes with actin-rich structures such as filopodia, lamellipodia and focal adhesion points, thereby regulating cell morphology and net movement of neurites (Goswami *et al.*, 2010). Taken together, we present pharmacological evidence demonstrating that TRPV4 inhibition is correlated with reduced cytoskeleton remodeling.

In our experiments, the constitutive absence of functional TRPV4 failed to alter microglia morphology and displacement *in vitro*. Although this is contradiction with previous results showing reduced microglial migration in *Trpv4* KO microglia (Nishimoto *et al.*, 2021), there are important differences regarding mouse age, isolation protocol and culture conditions to consider. Unlike previous *in vitro* results using *Trpv4* KO microglia, we isolate microglia from postnatal day 21 mice, an age when murine microglia have acquired their mature transcriptomic signature (Bennett *et al.*, 2016;

Matcovitch-Natan *et al.*, 2016). For these cultures, substrate coating is essential for cell survival and the development of morphological features and dynamics that mimics resting microglia (Bohlen *et al.*, 2017). In this condition, cultured microglia are sensitive to topological and mechanical properties of the substrate (Bollmann *et al.*, 2015), likely involving redundant intracellular signaling from mechanosensitive channels. This includes several other Ca^{2+}-permeable channels involved in cell migration. For instance, TRPM7 and TRPM2 are correlated with Ca^{2+}-driven cell movement (Almasi *et al.*, 2019; Jiang *et al.*, 2003; Nishimoto *et al.*, 2021; Wei *et al.*, 2009), and mechanically-gated Piezo channels with a pivotal role in cell migration by regulating actin structures and modifying cell shape through cation influx (Canales Coutino & Mayor, 2021; Mousawi *et al.*, 2020). We found that TRPM2, TRPM7 and Piezo channels are not differentially-regulated in *Trpv4* KO microglia (**Figure S4**). Our results indicate that the basal expression of these channels is sufficient to compensate for the constitutive lack of TRPV4, but not for the immediate, acute inhibition of TRPV4. Altogether, these findings suggest that, although the functional TRPV4 activity might be redundant, it outbalances other Ca^{2+}-permeable channels in the homeostatic regulation of cytoskeletal dynamism.

Microglia within the brain parenchyma interact with a vast diversity of extracellular matrix components present in the perineural nets (e.g. proteoglycan, tenascin R) and the neural interstitial matrix (e.g. collagen, fibronectin, laminin) predominantly through GPCR and integrin receptors, both acting as endogenous modulators of TRPV4 activity (Matthews *et al.*, 2010; Saifeddine *et al.*, 2015). This might increase the specific dependence of TRPV4 signaling, resulting in the reduced ramifications, shorter branches and less branching points observed *in situ*.

It should be noted that microglia can sense and respond to changes in neuronal activity (Umpierre *et al.*, 2020; Umpierre & Wu, 2021) and that neuronal cells express TRPV4 on their plasma membrane (Goswami *et al.*, 2010; Kanju & Liedtke, 2016). Therefore, the absence of TRPV4 in microglial cells may be influenced by the overall lack of TRPV4 in other brain cells. Yet, our *in vitro* experiments prove a cell-autonomous role for TRPV4 in microglia. Alternative approaches such as the Cre-Lox system or a bone marrow chimera (Cronk *et al.*, 2018) with microglia-specific *Trpv4* deficiency could provide supportive information regarding microglia cell-specific effects.

In conclusion, our results demonstrate that the mechanosensitive Ca^{2+}-permeable channel TRPV4 contributes to the regulation of the actin and MT cytoskeleton in microglia consequently steering morphological complexity and movement of the cells. The significance of this research is substantial as it provides novel insights into the link between cytoskeletal dynamism and ion channels in microglial properties and hereby contributes to unravelling cellular and molecular mechanisms underpinning proper microglial function.

5. REFERENCES

Almasi, S., Sterea, A. M., Fernando, W., Clements, D. R., Marcato, P., Hoskin, D. W., Gujar, S., & El Hiani, Y. (2019). TRPM2 ion channel promotes gastric cancer migration, invasion and tumor growth through the AKT signaling pathway. *Sci Rep, 9*(1), 4182. doi:10.1038/s41598-019-40330-1

Becker, D., Blase, C., Bereiter-Hahn, J., & Jendrach, M. (2005). TRPV4 exhibits a functional role in cell-volume regulation. *J Cell Sci, 118*(Pt 11), 2435-2440. doi:10.1242/jcs.02372

Bennett, M. L., Bennett, F. C., Liddelow, S. A., Ajami, B., Zamanian, J. L., Fernhoff, N. B., Mulinyawe, S. B., Bohlen, C. J., Adil, A., Tucker, A., Weissman, I. L., Chang, E. F., Li, G., Grant, G. A., Hayden Gephart, M. G., & Barres, B. A. (2016). New tools for studying microglia in the mouse and human CNS. *Proc Natl Acad Sci U S A, 113*(12), E1738-1746. doi:10.1073/pnas.1525528113

Bernier, L. P., Bohlen, C. J., York, E. M., Choi, H. B., Kamyabi, A., Dissing-Olesen, L., Hefendehl, J. K., Collins, H. Y., Stevens, B., Barres, B. A., & MacVicar, B. A. (2019). Nanoscale Surveillance of the Brain by Microglia via cAMP-Regulated Filopodia. *Cell Rep, 27*(10), 2895-2908 e2894. doi:10.1016/j.celrep.2019.05.010

Bohlen, C. J., Bennett, F. C., Tucker, A. F., Collins, H. Y., Mulinyawe, S. B., & Barres, B. A. (2017). Diverse Requirements for Microglial Survival, Specification, and Function Revealed by Defined-Medium Cultures. *Neuron, 94*(4), 759-773 e758. doi:10.1016/j.neuron.2017.04.043

Bollmann, L., Koser, D. E., Shahapure, R., Gautier, H. O., Holzapfel, G. A., Scarcelli, G., Gather, M. C., Ulbricht, E., & Franze, K. (2015). Microglia mechanics: immune activation alters traction forces and durotaxis. *Front Cell Neurosci, 9*, 363. doi:10.3389/fncel.2015.00363

Canales Coutino, B., & Mayor, R. (2021). Mechanosensitive ion channels in cell migration. *Cells Dev, 166*, 203683. doi:10.1016/j.cdev.2021.203683

Canales, J., Morales, D., Blanco, C., Rivas, J., Diaz, N., Angelopoulos, I., & Cerda, O. (2019). A TR(i)P to Cell Migration: New Roles of TRP Channels in Mechanotransduction and Cancer. *Front Physiol, 10*, 757. doi:10.3389/fphys.2019.00757

Chakraborty, R., & Goswami, C. (2022). Both heat-sensitive TRPV4 and cold-sensitive TRPM8 ion channels regulate microglial activity. *Biochem Biophys Res Commun, 611*, 132-139. doi:10.1016/j.bbrc.2022.04.032

Clapham, D. E. (2003). TRP channels as cellular sensors. *Nature, 426*(6966), 517-524. doi:10.1038/nature02196

Colonna, M., & Butovsky, O. (2017). Microglia Function in the Central Nervous System During Health and Neurodegeneration. *Annu Rev Immunol, 35*, 441-468. doi:10.1146/annurev-immunol-051116-052358

Cronk, J. C., Filiano, A. J., Louveau, A., Marin, I., Marsh, R., Ji, E., Goldman, D. H., Smirnov, I., Geraci, N., Acton, S., Overall, C. C., & Kipnis, J. (2018). Peripherally derived macrophages can engraft the brain independent of irradiation and maintain an identity distinct from microglia. *J Exp Med, 215*(6), 1627-1647. doi:10.1084/jem.20180247

Dutta, B., Arya, R. K., Goswami, R., Alharbi, M. O., Sharma, S., & Rahaman, S. O. (2020). Role of macrophage TRPV4 in inflammation. *Lab Invest, 100*(2), 178-185. doi:10.1038/s41374-019-0334-6

Echeverry, S., Rodriguez, M. J., & Torres, Y. P. (2016). Transient Receptor Potential Channels in Microglia: Roles in Physiology and Disease. *Neurotox Res, 30*(3), 467-478. doi:10.1007/s12640-016-9632-6

Eyo, U. B., Peng, J., Swiatkowski, P., Mukherjee, A., Bispo, A., & Wu, L. J. (2014). Neuronal hyperactivity recruits microglial processes via neuronal NMDA receptors and microglial P2Y12 receptors after status epilepticus. *J Neurosci, 34*(32), 10528-10540. doi:10.1523/JNEUROSCI.0416-14.2014

Franco-Bocanegra, D. K., McAuley, C., Nicoll, J. A. R., & Boche, D. (2019). Molecular Mechanisms of Microglial Motility: Changes in Ageing and Alzheimer's Disease. *Cells, 8*(6). doi:10.3390/cells8060639

Gallop, J. L. (2020). Filopodia and their links with membrane traffic and cell adhesion. *Semin Cell Dev Biol, 102*, 81-89. doi:10.1016/j.semcdb.2019.11.017

514 Goswami, C., Kuhn, J., Heppenstall, P. A., & Hucho, T. (2010). Importance of non-selective cation
515 channel TRPV4 interaction with cytoskeleton and their reciprocal regulations in cultured cells. *PLoS*
516 *One, 5*(7), e11654. doi:10.1371/journal.pone.0011654

517 Haynes, S. E., Hollopeter, G., Yang, G., Kurpius, D., Dailey, M. E., Gan, W. B., & Julius, D. (2006).
518 The P2Y12 receptor regulates microglial activation by extracellular nucleotides. *Nat Neurosci,*
519 *9*(12), 1512-1519. doi:10.1038/nn1805

520 Hines, D. J., Hines, R. M., Mulligan, S. J., & Macvicar, B. A. (2009). Microglia processes block the
521 spread of damage in the brain and require functional chloride channels. *Glia, 57*(15), 1610-1618.
522 doi:10.1002/glia.20874

523 Jiang, X., Newell, E. W., & Schlichter, L. C. (2003). Regulation of a TRPM7-like current in rat brain
524 microglia. *J Biol Chem, 278*(44), 42867-42876. doi:10.1074/jbc.M304487200

525 Jung, S., Aliberti, J., Graemmel, P., Sunshine, M. J., Kreutzberg, G. W., Sher, A., & Littman, D. R.
526 (2000). Analysis of fractalkine receptor CX(3)CR1 function by targeted deletion and green
527 fluorescent protein reporter gene insertion. *Mol Cell Biol, 20*(11), 4106-4114.
528 doi:10.1128/MCB.20.11.4106-4114.2000

529 Kanju, P., & Liedtke, W. (2016). Pleiotropic function of TRPV4 ion channels in the central nervous
530 system. *Exp Physiol, 101*(12), 1472-1476. doi:10.1113/EP085790

531 Konno, M., Shirakawa, H., Iida, S., Sakimoto, S., Matsutani, I., Miyake, T., Kageyama, K.,
532 Nakagawa, T., Shibasaki, K., & Kaneko, S. (2012). Stimulation of transient receptor potential
533 vanilloid 4 channel suppresses abnormal activation of microglia induced by lipopolysaccharide. *Glia,*
534 *60*(5), 761-770. doi:10.1002/glia.22306

535 Kyrargyri, V., Madry, C., Rifat, A., Arancibia-Carcamo, I. L., Jones, S. P., Chan, V. T. T., Xu, Y.,
536 Robaye, B., & Attwell, D. (2020). P2Y13 receptors regulate microglial morphology, surveillance,
537 and resting levels of interleukin 1beta release. *Glia, 68*(2), 328-344. doi:10.1002/glia.23719

538 Li, X., Cheng, Y., Wang, Z., Zhou, J., Jia, Y., He, X., Zhao, L., Dong, Y., Fan, Y., Yang, X., Shen, B.,
539 Wu, X., Wang, J., Xiong, C., Wei, L., Li, X., & Wang, J. (2020). Calcium and TRPV4 promote
540 metastasis by regulating cytoskeleton through the RhoA/ROCK1 pathway in endometrial cancer.
541 *Cell Death Dis, 11*(11), 1009. doi:10.1038/s41419-020-03181-7

542 Liu, C., & Montell, C. (2015). Forcing open TRP channels: Mechanical gating as a unifying activation
543 mechanism. *Biochem Biophys Res Commun, 460*(1), 22-25. doi:10.1016/j.bbrc.2015.02.067

544 Madry, C., & Attwell, D. (2015). Receptors, ion channels, and signaling mechanisms underlying
545 microglial dynamics. *J Biol Chem, 290*(20), 12443-12450. doi:10.1074/jbc.R115.637157

546 Matcovitch-Natan, O., Winter, D. R., Giladi, A., Vargas Aguilar, S., Spinrad, A., Sarrazin, S., Ben-
547 Yehuda, H., David, E., Zelada Gonzalez, F., Perrin, P., Keren-Shaul, H., Gury, M., Lara-Astaiso, D.,
548 Thaiss, C. A., Cohen, M., Bahar Halpern, K., Baruch, K., Deczkowska, A., Lorenzo-Vivas, E.,
549 Itzkovitz, S., Elinav, E., Sieweke, M. H., Schwartz, M., & Amit, I. (2016). Microglia development
550 follows a stepwise program to regulate brain homeostasis. *Science, 353*(6301), aad8670.
551 doi:10.1126/science.aad8670

552 Matthews, B. D., Thodeti, C. K., Tytell, J. D., Mammoto, A., Overby, D. R., & Ingber, D. E. (2010).
553 Ultra-rapid activation of TRPV4 ion channels by mechanical forces applied to cell surface beta1
554 integrins. *Integr Biol (Camb), 2*(9), 435-442. doi:10.1039/c0ib00034e

555 Meijering, E., Dzyubachyk, O., & Smal, I. (2012). Methods for cell and particle tracking. *Methods*
556 *Enzymol, 504*, 183-200. doi:10.1016/B978-0-12-391857-4.00009-4

557 Michalick, L., & Kuebler, W. M. (2020). TRPV4-A Missing Link Between Mechanosensation and
558 Immunity. *Front Immunol, 11*, 413. doi:10.3389/fimmu.2020.00413

559 Mizoguchi, Y., Kato, T. A., Seki, Y., Ohgidani, M., Sagata, N., Horikawa, H., Yamauchi, Y., Sato-
560 Kasai, M., Hayakawa, K., Inoue, R., Kanba, S., & Monji, A. (2014). Brain-derived neurotrophic
561 factor (BDNF) induces sustained intracellular Ca2+ elevation through the up-regulation of surface
562 transient receptor potential 3 (TRPC3) channels in rodent microglia. *J Biol Chem, 289*(26), 18549-
563 18555. doi:10.1074/jbc.M114.555334

564 Mousawi, F., Peng, H., Li, J., Ponnambalam, S., Roger, S., Zhao, H., Yang, X., & Jiang, L. H. (2020).
565 Chemical activation of the Piezo1 channel drives mesenchymal stem cell migration via inducing

ATP release and activation of P2 receptor purinergic signaling. *Stem Cells, 38*(3), 410-421. doi:10.1002/stem.3114

Nilius, B., & Owsianik, G. (2011). The transient receptor potential family of ion channels. *Genome Biol, 12*(3), 218. doi:10.1186/gb-2011-12-3-218

Nimmerjahn, A., Kirchhoff, F., & Helmchen, F. (2005). Resting microglial cells are highly dynamic surveillants of brain parenchyma in vivo. *Science, 308*(5726), 1314-1318. doi:10.1126/science.1110647

Nishimoto, R., Derouiche, S., Eto, K., Deveci, A., Kashio, M., Kimori, Y., Matsuoka, Y., Morimatsu, H., Nabekura, J., & Tominaga, M. (2021). Thermosensitive TRPV4 channels mediate temperature-dependent microglia movement. *Proc Natl Acad Sci U S A, 118*(17). doi:10.1073/pnas.2012894118

Ohsawa, K., & Kohsaka, S. (2011). Dynamic motility of microglia: purinergic modulation of microglial movement in the normal and pathological brain. *Glia, 59*(12), 1793-1799. doi:10.1002/glia.21238

Ou-Yang, Q., Li, B., Xu, M., & Liang, H. (2018). TRPV4 promotes the migration and invasion of glioma cells via AKT/Rac1 signaling. *Biochem Biophys Res Commun, 503*(2), 876-881. doi:10.1016/j.bbrc.2018.06.090

Redmon, S. N., Yarishkin, O., Lakk, M., Jo, A., Mustafic, E., Tvrdik, P., & Krizaj, D. (2021). TRPV4 channels mediate the mechanoresponse in retinal microglia. *Glia, 69*(6), 1563-1582. doi:10.1002/glia.23979

Ryskamp, D. A., Frye, A. M., Phuong, T. T., Yarishkin, O., Jo, A. O., Xu, Y., Lakk, M., Iuso, A., Redmon, S. N., Ambati, B., Hageman, G., Prestwich, G. D., Torrejon, K. Y., & Krizaj, D. (2016). TRPV4 regulates calcium homeostasis, cytoskeletal remodeling, conventional outflow and intraocular pressure in the mammalian eye. *Sci Rep, 6*, 30583. doi:10.1038/srep30583

Saifeddine, M., El-Daly, M., Mihara, K., Bunnett, N. W., McIntyre, P., Altier, C., Hollenberg, M. D., & Ramachandran, R. (2015). GPCR-mediated EGF receptor transactivation regulates TRPV4 action in the vasculature. *Br J Pharmacol, 172*(10), 2493-2506. doi:10.1111/bph.13072

Salter, M. W., & Stevens, B. (2017). Microglia emerge as central players in brain disease. *Nat Med, 23*(9), 1018-1027. doi:10.1038/nm.4397

Sappington, R. M., & Calkins, D. J. (2008). Contribution of TRPV1 to microglia-derived IL-6 and NFkappaB translocation with elevated hydrostatic pressure. *Invest Ophthalmol Vis Sci, 49*(7), 3004-3017. doi:10.1167/iovs.07-1355

Schiefer, J., Kampe, K., Dodt, H. U., Zieglgansberger, W., & Kreutzberg, G. W. (1999). Microglial motility in the rat facial nucleus following peripheral axotomy. *J Neurocytol, 28*(6), 439-453. doi:10.1023/a:1007048903862

Schindelin, J., Arganda-Carreras, I., Frise, E., Kaynig, V., Longair, M., Pietzsch, T., Preibisch, S., Rueden, C., Saalfeld, S., Schmid, B., Tinevez, J. Y., White, D. J., Hartenstein, V., Eliceiri, K., Tomancak, P., & Cardona, A. (2012). Fiji: an open-source platform for biological-image analysis. *Nat Methods, 9*(7), 676-682. doi:10.1038/nmeth.2019

Sharma, P., & Ping, L. (2014). Calcium ion influx in microglial cells: physiological and therapeutic significance. *J Neurosci Res, 92*(4), 409-423. doi:10.1002/jnr.23344

Smolders, S. M., Kessels, S., Vangansewinkel, T., Rigo, J. M., Legendre, P., & Brone, B. (2019). Microglia: Brain cells on the move. *Prog Neurobiol, 178*, 101612. doi:10.1016/j.pneurobio.2019.04.001

Stark, J. C., Wallace, E., Lim, R., & Leaw, B. (2018). Characterization and Isolation of Mouse Primary Microglia by Density Gradient Centrifugation. *J Vis Exp*(132). doi:10.3791/57065

Sun, Y., Chauhan, A., Sukumaran, P., Sharma, J., Singh, B. B., & Mishra, B. B. (2014). Inhibition of store-operated calcium entry in microglia by helminth factors: implications for immune suppression in neurocysticercosis. *J Neuroinflammation, 11*, 210. doi:10.1186/s12974-014-0210-7

Swiatkowski, P., Murugan, M., Eyo, U. B., Wang, Y., Rangaraju, S., Oh, S. B., & Wu, L. J. (2016). Activation of microglial P2Y12 receptor is required for outward potassium currents in response to neuronal injury. *Neuroscience, 318*, 22-33. doi:10.1016/j.neuroscience.2016.01.008

Thevenaz, P., Ruttimann, U. E., & Unser, M. (1998). A pyramid approach to subpixel registration based on intensity. *IEEE Trans Image Process, 7*(1), 27-41. doi:10.1109/83.650848

Thielicke, W., & Stamhuis, E. J. (2014). PIVlab – Towards User-friendly, Affordable and Accurate Digital Particle Image Velocimetry in MATLAB. *J. Open Res. Softw., 2*(1), p.e30. doi: http://doi.org/10.5334/jors.bl

Tsai, F. C., Kuo, G. H., Chang, S. W., & Tsai, P. J. (2015). Ca2+ signaling in cytoskeletal reorganization, cell migration, and cancer metastasis. *Biomed Res Int, 2015*, 409245. doi:10.1155/2015/409245

Tsai, F. C., & Meyer, T. (2012). Ca2+ pulses control local cycles of lamellipodia retraction and adhesion along the front of migrating cells. *Curr Biol, 22*(9), 837-842. doi:10.1016/j.cub.2012.03.037

Umpierre, A. D., Bystrom, L. L., Ying, Y., Liu, Y. U., Worrell, G., & Wu, L. J. (2020). Microglial calcium signaling is attuned to neuronal activity in awake mice. *Elife, 9*. doi:10.7554/eLife.56502

Umpierre, A. D., & Wu, L. J. (2021). How microglia sense and regulate neuronal activity. *Glia, 69*(7), 1637-1653. doi:10.1002/glia.23961

Wei, C., Wang, X., Chen, M., Ouyang, K., Song, L. S., & Cheng, H. (2009). Calcium flickers steer cell migration. *Nature, 457*(7231), 901-905. doi:10.1038/nature07577

Wolf, S. A., Boddeke, H. W., & Kettenmann, H. (2017). Microglia in Physiology and Disease. *Annu Rev Physiol, 79*, 619-643. doi:10.1146/annurev-physiol-022516-034406

Xiao, H., & Peng, H. (2013). APP2: automatic tracing of 3D neuron morphology based on hierarchical pruning of a gray-weighted image distance-tree. *Bioinformatics, 29*(11), 1448-1454. doi:10.1093/bioinformatics/btt170

642 **FIGURE LEGENDS**

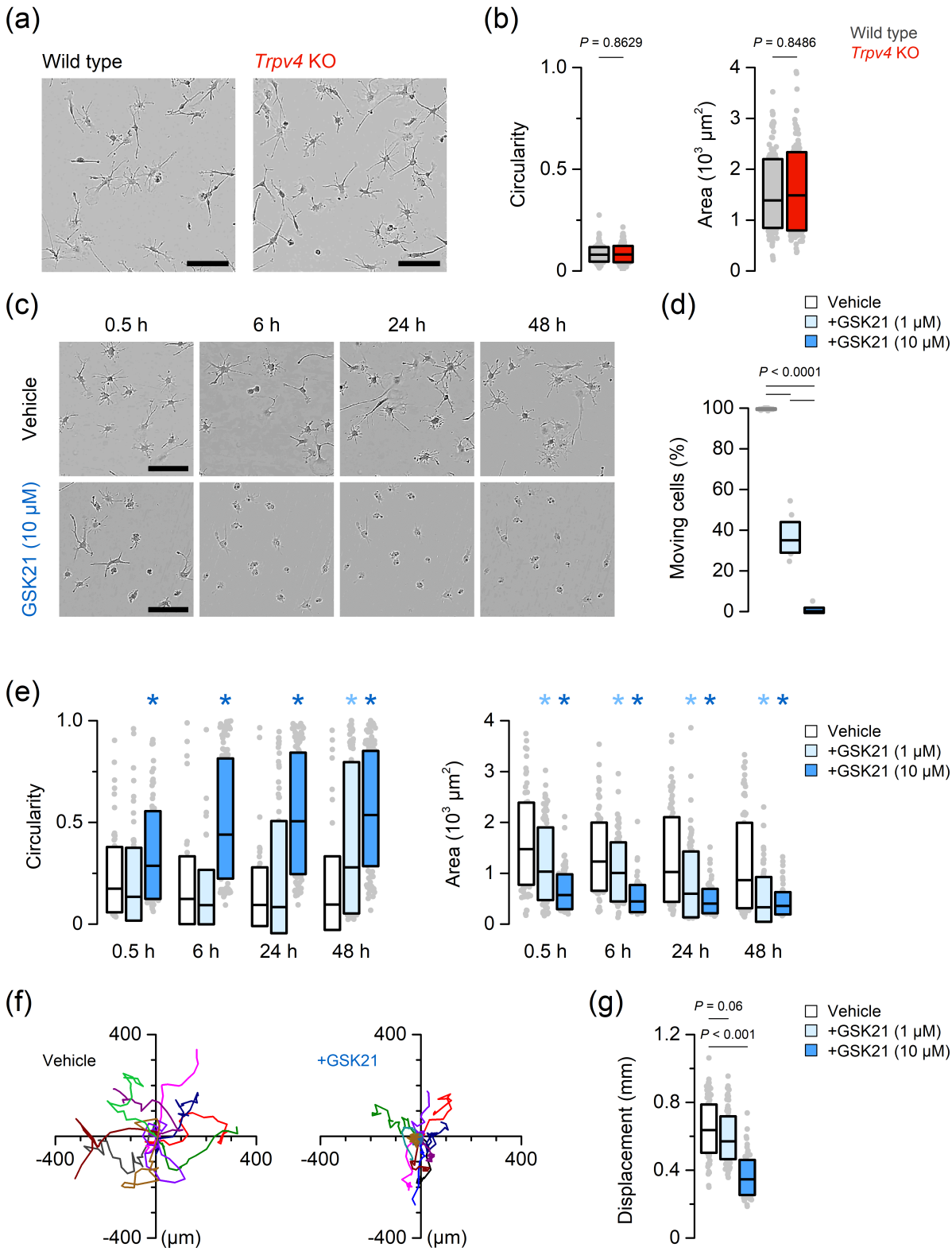

643

644 **FIGURE 1** Acute inhibition of TRPV4 triggers morphological and migratory changes on primary microglia *in vitro*.

645 (a) Representative brightfield images of WT and *Trpv4* KO primary microglia after 7 days in culture in collagen-

coated plates with TIC medium. Scale bar, 100 µm. (b) Circularity and area from WT and *Trpv4* KO microglia were analyzed using Fiji software. Quantification revealed no morphological differences between both genotypes (n ≥ 150 per genotype, two-tailed Mann-Whitney *U* test). (c) Representative brightfield images of WT primary microglia at different time points after addition of vehicle (0.2% DMSO) or GSK21 (10 µM). Scale bar, 100 µm. (d) Percentage of actively moving microglia 24 h after incubation with vehicle or GSK21 (1 µM and 10 µM). Data points (16 per condition, n ≥ 1300 cells) represent one quantified field of view (FOV, 1745 x 1289 µm). FOVs were randomly selected from different wells from at least 2 independent experiments. $P < 0.0001$ for all paired comparisons, two-tailed Fisher's exact test. (e) Circularity and area parameters on primary microglia after acute inhibition of TRPV4 (GSK21, 1 µM and 10 µM). Asterisks indicate statistically significant differences (of at least $P < 0.05$) to the untreated cells (Vehicle). Two-tailed Dunn's multiple comparison test, n ≥ 100 per condition. Exact *P* values for all paired comparison are listed in **Table S1**. (f) Representative persistent random walk traces of WT microglia untreated and treated with the TRPV4 inhibitor (GSK21, 10 µM). (g) Total displacement in 24 h during persistent random walk of untreated and GSK21-treated (1 µM and 10 µM) primary microglia. Two-tailed Dunn's multiple comparison test, n ≥ 92 cells per condition.

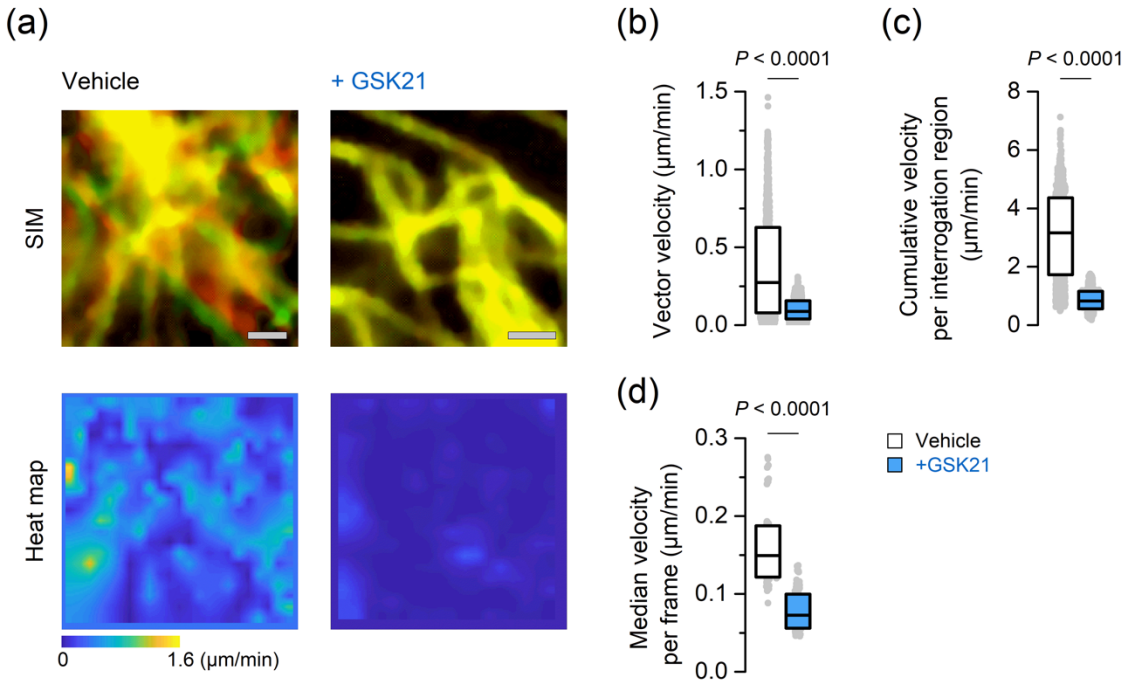

FIGURE 2 Dynamism of microglial tubulin decreases upon pharmacological inhibition of TRPV4. (a) Representative structure illumination microscopy (SIM) images of tubulin structures (upper panel) recorded in WT and TRPV4-inhibited (GSK21) microglia. Green and red colours represent two consecutive images taken 5 sec apart. Scale bar, 1 µm. PIVlab-generated heat maps of particle vector velocity calculation are shown below the corresponding SIM image. The colour-coded bar indicates the range of vector velocity magnitude. (b) Vector velocity values of all interrogation areas of the representative images for control and GSK21-treated microglia shown in (a). (c) Cumulative velocity values per interrogation area of the representative experiment during 1 min of recording. (d) Median vector velocity value per time frame. Data points represent individually analyzed images (n ≥ 153 regions per condition, from two independent experiments). (b-d) Two-tailed Mann Whitney *U* test.

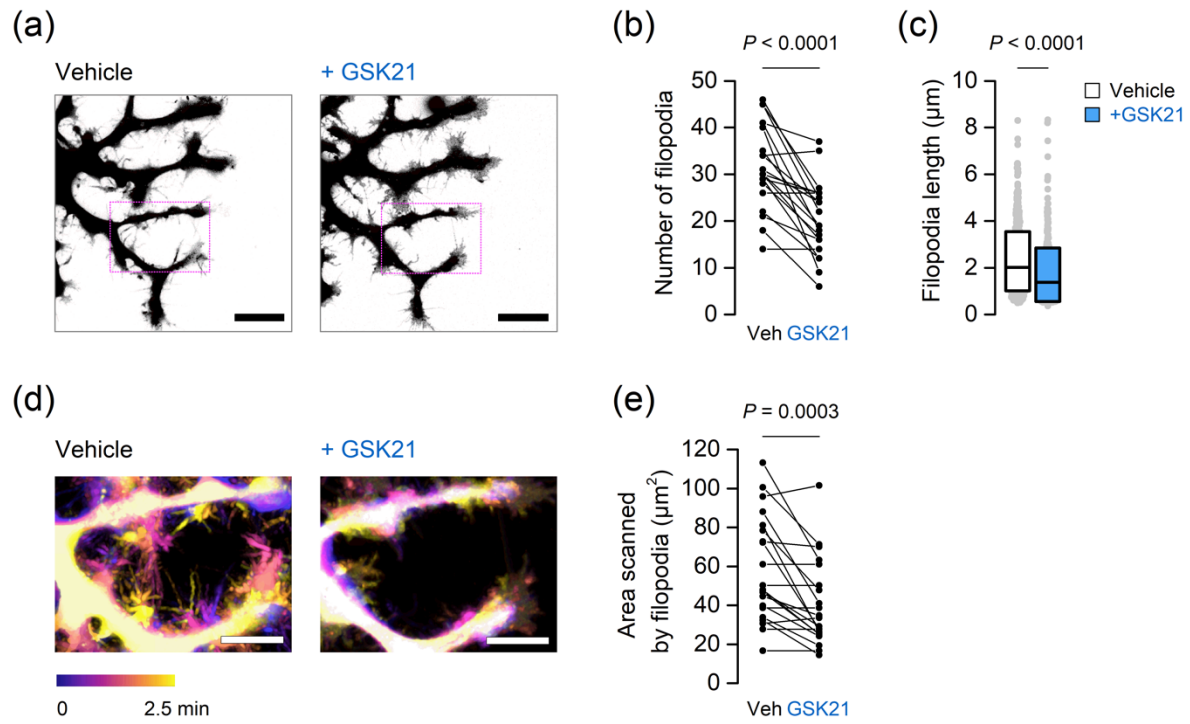

673

674 **FIGURE 3** Acute inhibition of TRPV4 affects length and motility of actin-rich filopodia in microglia. (a)
675 Representative Airyscan images of selected regions in untreated and GSK21-treated microglia. The selection in
676 magenta corresponds to the image shown in (d). Scale bar, 10 µm. (b) Number of filopodia during incubation
677 with vehicle (0.2% DMSO) and after acute inhibition of TRPV4 (GSK21). Data points represent individual regions
678 (n = 21) from 5 cells. Wilcoxon matched-pairs signed rank test. (c) Length of filopodia before (0.2% DMSO,
679 Vehicle) and after acute inhibition of TRPV4 (GSK21). Data points represent individual filopodia (n ≥ 430). Two-
680 tailed Mann Whitney *U* test. (d) Temporal colour-coded overlaid images of the area represented in (a) (magenta
681 rectangle) for microglia before and after acute inhibition of TRPV4. The colour-coded bar indicates the time range.
682 Scale bar embedded, 5 µm. (e) Total scanned area by filopodia in selected regions (n = 21; 5 cells). Wilcoxon
683 matched-pairs signed rank test.

684

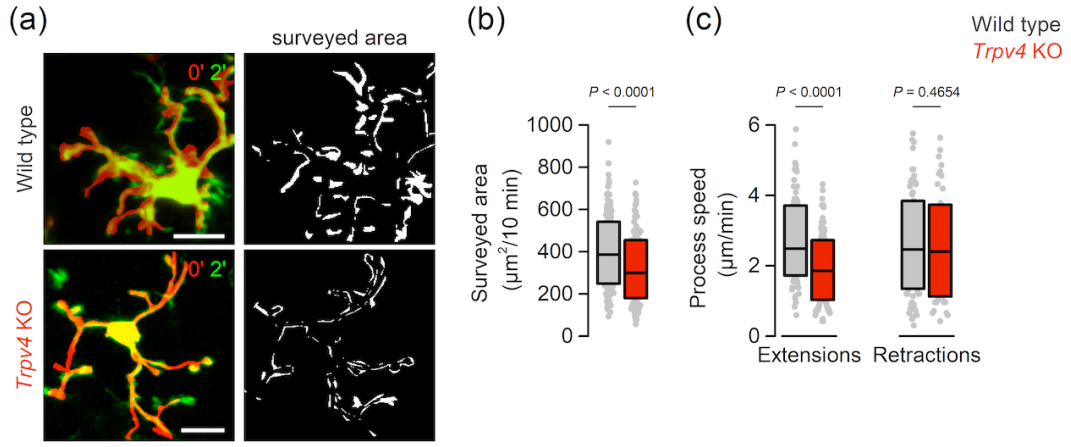

685
686 **FIGURE 4** Constitutive absence of TRPV4 affects microglial brain surveillance *in situ*. (a) Representative two-
687 photon microscopy images of CX3CR1$^{eGFP/+}$ WT and *Trpv4* KO cortical microglia in acute brain slices. Images taken
688 2 min apart are overlaid with two different colours (red: 0 min, green: 2 min). Scale bar, 10 μm. The panels on
689 the right represent the difference between the two images (2'(green) – 0'(red)). (b) Total surveyed area by
690 CX3CR1$^{eGFP/+}$ WT (n = 211 cells) and *Trpv4* KO (n = 179 cells) cortical microglia in acute brain slices. (c) Speed
691 of process extension and retraction events in CX3CR1$^{eGFP/+}$ WT and *Trpv4* KO cortical microglia. The speed of
692 extension (n ≥ 139 per genotype) and retraction (n ≥ 69 per genotype) events were quantified from at least 5
693 independent slices/mice. (b, c) Two-tailed Mann Whitney *U* test.
694

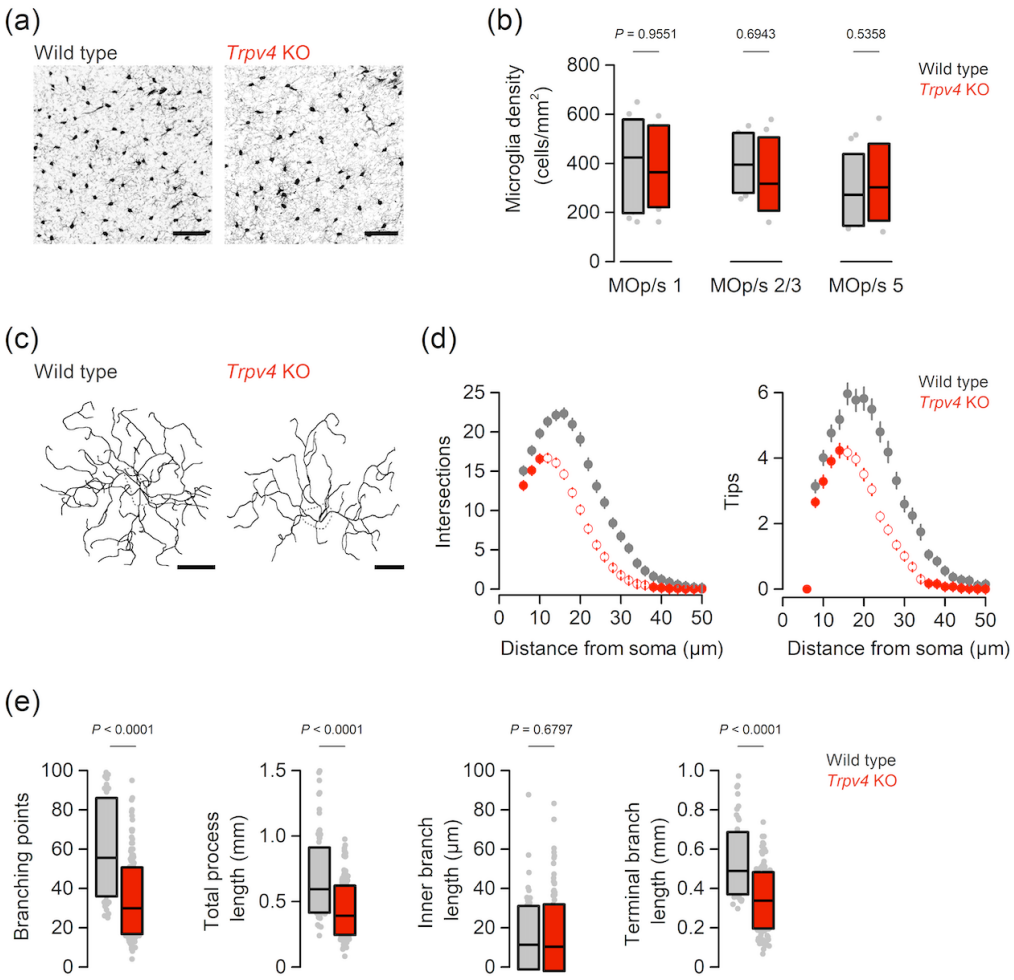

FIGURE 5 *Trpv4* KO microglia exhibit decreased branch ramifications *in situ*. (a) Representative confocal images of perfusion-fixed P21 CX3CR1$^{eGFP/+}$ WT and *Trpv4* KO cortical brain slices. Scale bar, 50 µm. (b) Average microglial density in layer 1, 2/3 and 5 of the primary and secondary motor areas (MOp/s) of the cortex from CX3CR1$^{eGFP/+}$ WT (n = 8) and *Trpv4* KO (n = 7) brains. (c) Representative 3D skeletonized microglia obtained from P21 CX3CR1$^{eGFP/+}$ WT and *Trpv4* KO mice. The dotted line represents the somatic area. Scale bar, 10 µm. (d, e) Ramification analysis of microglia from perfusion-fixed WT (112 cells, 5 animals) and *Trpv4* KO (193 cells, 5 animals) mice showing Sholl analysis-derived average number of process intersections and tips (d), and number of branching points, total process length, inner branch length and terminal branch length (e) per individual microglia. Empty data points in (d) indicate significant differences ($P < 0.0001$, multiple Mann-Whitney *U* test) from equidistant value in WT. Data in (d) are represented as mean ± SEM. (b, e) Two-tailed Mann Whitney *U* test.

SUPPLEMENTARY INFORMATION

Acute inhibition of transient receptor potential vanilloid-type 4 cation channel halts cytoskeletal dynamism in microglia.

Jolien Beeken, Melanie Mertens, Nathan Stas, Sofie Kessels, Liese Aerts, Bieke Janssen, Femke Mussen, Silvia Pinto, Rudi Vennekens, Jean-Michel Rigo, Laurent Nguyen, Bert Brône, Yeranddy A. Alpizar

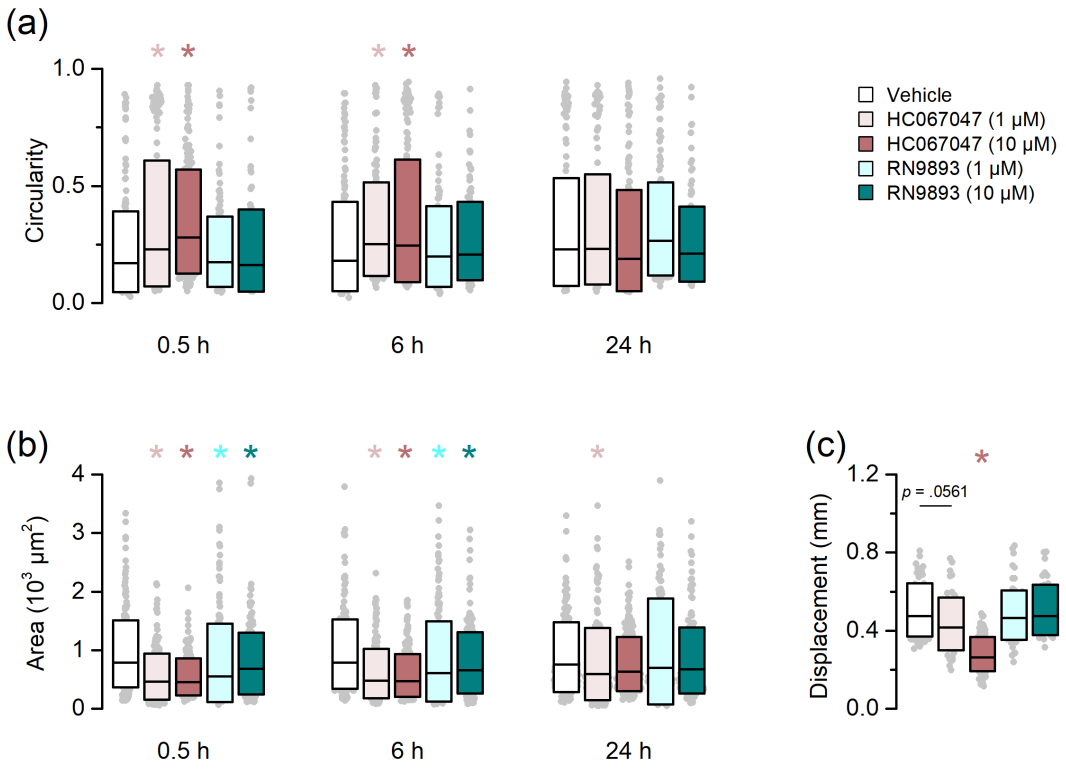

Figure S1: Differential effects of TRPV4 inhibitors on the morphological and migratory changes on wild type microglia *in vitro*. (a, b) Circularity and area parameters on wild type primary microglia after acute inhibition of TRPV4 with HC067047 and RN9893 (n ≥ 202 per condition). (c) Total displacement in 6 h during persistent random walk in the presence of TRPV4 inhibitors. (n ≥ 62 cells per condition). Asterisks indicate statistically significant differences (of at least $p < .05$) with vehicle-treated cells (Vehicle, 0.2% DMSO); two-tailed Dunn's multiple comparison test.

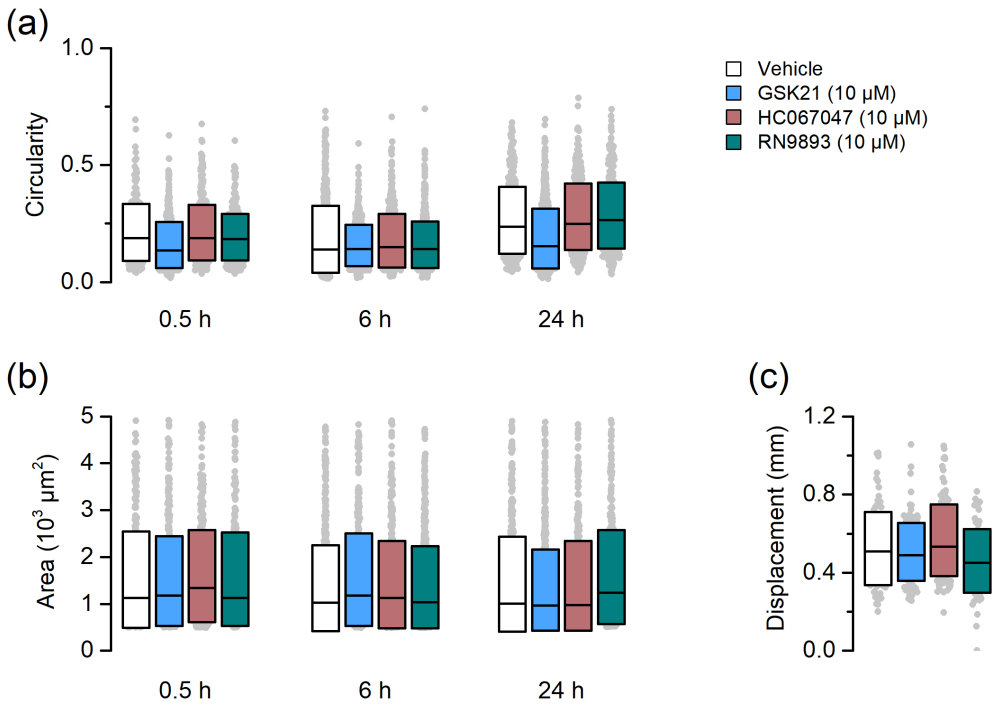

Figure S2: No off-target effects were induced by 3 different TRPV4 inhibitors on morphological and migratory parameters of TRPV4-deficient microglia *in vitro*. Statistical comparisons revealed no morphological differences compared to the vehicle-treated cells (n ≥ 162 per genotype, two-tailed Dunn's multiple comparison test). (c) Total displacement in 6 h during persistent random walk of *Trpv4* KO primary microglia treated with TRPV4 inhibitors. Two-tailed Dunn's multiple comparison test, n ≥ 67 cells per condition.

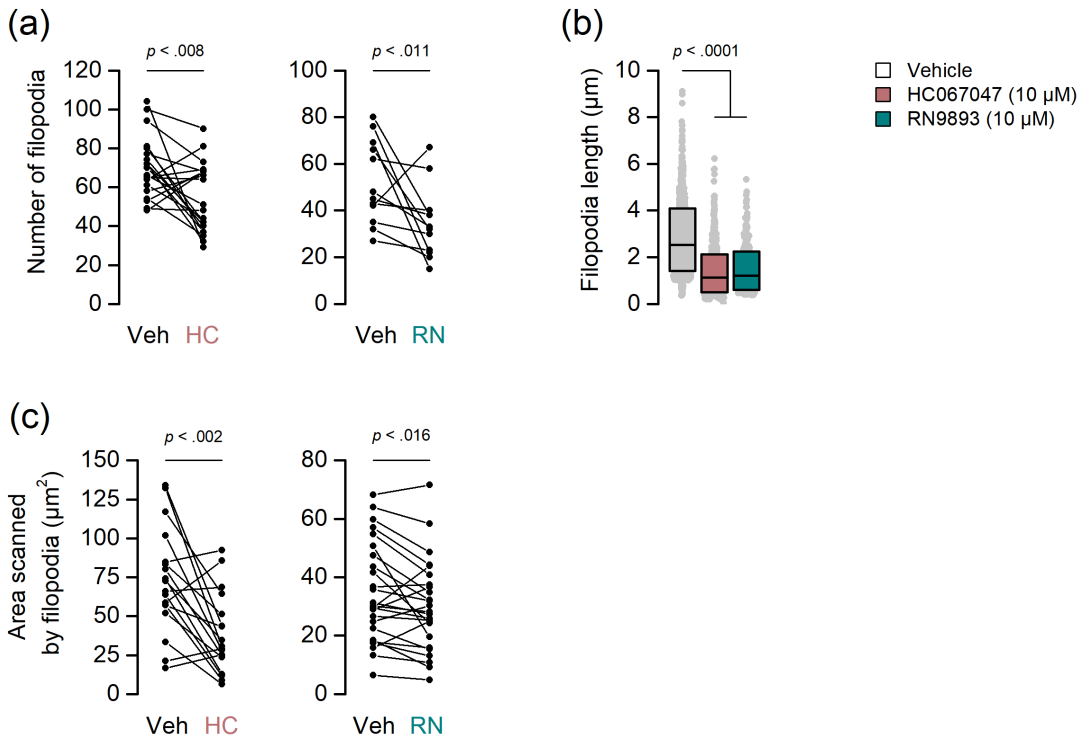

Figure S3: Acute inhibition of TRPV4 decreases length and motility of actin-rich filopodia in wild type microglia. (a) Number of filopodia during incubation with vehicle (0.2% DMSO) and after acute inhibition of TRPV4 (HC067047, RN9893). Data points represent individual regions (n_{HC} = 20, n_{RN} = 12) from 5 cells. Wilcoxon matched-pairs signed rank test. (b) Length of filopodia before (0.2% DMSO, Vehicle) and after acute inhibition of TRPV4. Data points represent individual filopodia (n ≥ 416 per condition). Two-tailed Mann Whitney *U* test. (c) Total scanned area by filopodia in selected regions (n_{HC} = 18, n_{RN} = 25; 8 cells). Wilcoxon matched-pairs signed rank test.

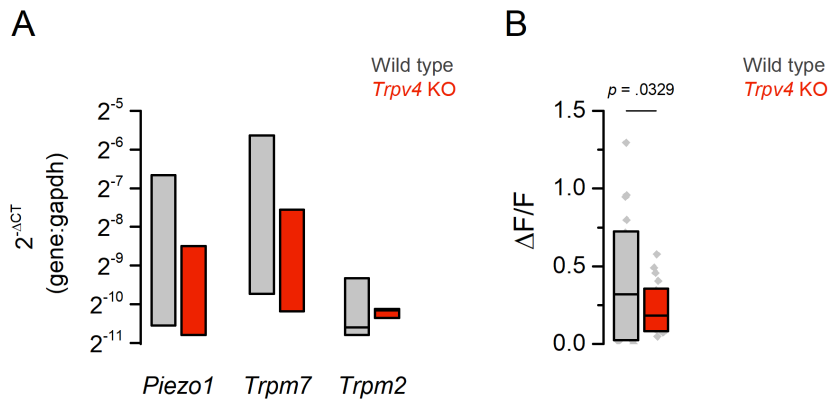

Figure S4: Expression profile of *Piezo1*, *Trpm7* and *Trpm2* in microglia of *Trpv4* KO mice. (a) Relative mRNA expression of *Piezo1*, *Trpm7 and Trpm2* in wild type and *Trpv4* KO microglia. Boxes represent the median and SD of delta Ct values, normalized to *Gapdh* expression (n = 3 mice per genotype). (b) Maximum amplitudes of intracellular Ca^{2+} levels in response to Yoda-1 (10 µM) recorded in wild type and *Trpv4* KO conditions. Boxes represent mean ± SD; Mann-Whitney *U* test.

Table S1.

P values for paired comparisons (Dunn's multiple comparison test) of data shown in Figure 1e.

	0.5 h			6 h			24 h			48 h			
	Ctrl	1 µM	10 µM	Ctrl	1 µM	10 µM	Ctrl	1 µM	10 µM	Ctrl	1 µM	10 µM	
Ctrl		**0.0023**	**<0.0001**		**0.0098**	**<0.0001**		**<0.0001**	**<0.0001**		**<0.0001**	**<0.0001**	Area
1 µM	0.1720		**<0.0001**	0.2911		**<0.0001**	>0.9999		**0.0010**	**<0.0001**		>0.9999	
10 µM	**0.0001**	**<0.0001**		**<0.0001**	**<0.0001**		**<0.0001**	**<0.0001**		**<0.0001**	**<0.0001**		
	Circularity												

Supplementary movie 1: Representative video showing highly dynamic microtubules in WT microglia over a timespan of 2.5 min.

Supplementary movie 2: Acute inhibition of TRPV4 drastically decreases tubulin dynamics.

Supplementary movie 3: Filopodia movement before and after treatment with the TRPV4 antagonist.

SUPPLEMENTARY METHODS

Quantitative real-time PCR

RNA was isolated from freshly-isolated CD11b^{+} cells extracted from WT and *Trpv4*$^{-/-}$ P21 brains using the RNeasy Mini Kit (Qiagen, Germany) following manufacturer's instructions. cDNA was synthesized through reverse transcription with the qScript cDNA SuperMix (VWR, Radnor, US) and diluted to a final concentration of 5 ng/µl. The cDNA was amplified by real-time PCR on the StepOnePlus Real-Time PCR system (Applied Biosystems, Foster City, US) using the SYBR Green Master Mix (Applied Biosystems), probes for *Piezo1*, *Piezo2*, *Trpm7*, *Trpm2* and *Gapdh*. *Piezo2* was not detected after 40 cycles, data not shown. Custom-made (*Trpm2*) or commercially available (*Piezo1*, *Piezo2*, *Trpm7*) primers were purchased at Integrated DNA Technologies (Leuven, Belgium).

Trpm2 (fwd: 5'-ACAACCCTGAAGGACAGTGG-3'; rev: 5'-CATCACTAGCACCTCCAGCA-3')
Trpm7 (Mm.PT.58.13777605)
Piezo1 (Mm.PT.58.11048868)
Piezo2 (Mm.PT.58.30174298)

Live-cell Ca^{2+} imaging

TIC medium-cultured, WT and *Trpv4* KO microglia seeded in MatTek glass bottom were incubated with Fluo-4 (2 µM, Invitrogen, USA) for 30 min. Afterwards, cells were rinsed and imaged before and after being exposed to solutions containing Yoda-1 (10 µM, Tocris Bioscience, Bristol, United Kingdom) prepared in Krebs (in mM: 150 NaCl, 6 KCl, 10 HEPES, 10 glucose, 1.5 $CaCl_2$, 1 $MgCl_2$, pH 7.4) either manually or via perfusion by gravity using a multi-barrelled pipette tip. Time-lapse live-cell Ca^{2+} imaging was performed with Zeiss Elyra PS.1 widefield fluorescence microscope with a 488 nm excitation laser and a laser power of 1%. Images were captured at one frame per second using a PCO Edge 4.2 sCMOS camera connected with an Ander iXon+ 897 EMCCD camera at a magnification of 10x. Acquired images were processed with Fiji (ImageJ v2.0, Open source software). For each time point, the mean pixel intensity in the soma was calculated. The response amplitude was calculated and normalized by the average pixel intensity of the baseline.